Performance of GaAs Nanowire Array Solar Cells for Varying Incidence Angles

Omid Madani Ghahfarokhi, Nicklas Anttu, Lars Samuelson, and Ingvar Åberg

***Abstract*—Nanowire array solar cells show intrinsic light trapping and absorption enhancement properties due to the diffraction and optical resonances. Here, we report the effect of varying incidence angle on the performance of GaAs nanowire array solar cells. We provide experimental evidence that nanowire array solar cells are highly efficient at gathering diffuse or tilted incident light, even at very high incidence angles; hence, the performance of the nanowire solar cell is retained up to these high incident light angles. Specifically, the measured efficiency at an incidence angle of 60° is 95% of the efficiency at normal incidence. Moreover, our measurements show that a nonzero incidence angle is beneficial for wavelengths above 600 nm, which results in an efficiency improvement by 0.5% absolute points. This increase is so large that we even measure a small increase in absolute output power at 15° tilt, thus, more than fully compensating for the reduced incoming power over the cell with increasing tilt. We show how this gain arises from an enhanced absorption in the part of the nanowire with a high probability of charge extraction. Thus, nanowires show great promise for the delivery of high efficiency in practical nontracking positioning conditions, as well as under diffuse light illumination.**

***Index Terms*—Gallium arsenide, nanowires, photovoltaic cells, tilted illumination.**

I. Introduction

III–V SEMICONDUCTOR materials offer excellent properties for various types of optoelectronic applications including photovoltaics. In particular, GaAs is of great interest for single-junction solar cells due to its optimum bandgap relative to the 1-sun air mass 1.5 global (AM1.5G) spectrum [1]. So far, the highest single-junction solar cell efficiency under 1-sun illumination was achieved with a GaAs cell [2], [3]. The most conventional approach to fabricate GaAs planar structures is through metal–organic vapor phase epitaxy (MOVPE). However, the epitaxial growth of GaAs layers grown by MOVPE is expensive, due to the high cost of organometallic precursors, as well as the cost of the MOVPE reactor and the single-crystal GaAs substrate. Moreover, the use of precursors is inefficient in MOVPE [4]. These limitations have, until now, hindered the use of GaAs for 1-sun solar cell modules.

Nanowire (NW)-based solar cells are promising candidates for future solar cell applications due to their advantageous properties such as improved light trapping and reduced material need [5]–[10]. For example, the recent demonstration of aerotaxy, a substrate-less continuous growth system based on vapor–liquid–solid growth, could eliminate the need for a growth substrate, while at the same time increasing growth rates by orders of magnitude [11]. Furthermore, the NW geometry allows the absorption of more than 90% of the incident photons with energy above the bandgap when we choose appropriate geometrical parameters such as NW diameter, NW length, and array pitch [10], [12], [13]. Such geometry optimization leads to excellent wave-coupling and subwavelength optical concentration in NWs. As a result, the material consumption can be reduced by up to one order of magnitude, while the concentrated light improves the open-circuit voltage (V_{OC}) [5].

Recently, we demonstrated a record efficiency of 15.3% for GaAs NW-array-based solar cells [9]. In this study, we address the effect of the angle of incidence on the performance of GaAs NW array solar cells. First, the NW geometry introduces absorption properties beyond the simple Beer–Lambert law of exponential intensity decay with depth into the cell, in strong contrast with a conventional planar cell. Second, the probability to extract the photogenerated charge carriers depends on the axial position along the NWs. Third, with a tilted nonnormal incidence angle, we tend to increase the photogeneration rate in regions of high extraction probability. As an end result, NW array solar cells are highly efficient at gathering diffuse or tilted incident light even at very high angles of incidence; therefore, the efficiency of the NW array solar cell stays high until high incidence angles (up to 60° incidence). This demonstrates the potential of a fixed-installation NW array solar cell for delivering large power output during the cycle of illumination from sunrise to sunset, as well as during diffuse illumination conditions.

II. Experimental Details and Modeling Method

We have used GaAs (111)B substrates decorated with a square grid pattern of Au disks (with diameter of 160 nm and pitch of 500 nm), where the Au disks were used as catalyst material for GaAs NW growth. The NW growth was performed using MOVPE at a growth temperature of 400 °C. Trimethylgallium (TMGa) and arsine (AsH_3) were used as precursors for the GaAs NW growth. Diethyl zinc (DEZn) and tetraethyl tin (TESn) were used as dopant precursors to fabricate, respectively, p-type (nominally grown 200 nm in length with an estimated doping level of 5–10 $\times$ 10^{18} cm^{-3}) and n-type (nominally grown 250 nm in length and an estimated doping level of 1–3 $\times$ 10^{18} cm^{-3}) segments in a p-n axial geometry, with a nominally intrinsic 2350-nm-long segment in between. Following the p-n axial NW growth, the surfaces of the NWs were passivated by growing a

Manuscript received July 6, 2016; revised August 17, 2016; accepted August 26, 2016. Date of publication September 26, 2016; date of current version October 19, 2016. This work was supported by the European Union's Horizon 2020 research and innovation program under Grant 696519 and Grant 641023, as well as by the Swedish Energy Agency.

The authors are with Sol Voltaics AB, Lund 22363, Sweden (e-mail: omid.madani@solvoltaics.com; nicklas.a@solvoltaics.com; lars.samuelson@ftf.lth.se; ingvar.aberg@solvoltaics.com).

Color versions of one or more of the figures in this paper are available online at http://ieeexplore.ieee.org.

Digital Object Identifier 10.1109/JPHOTOV.2016.2604564

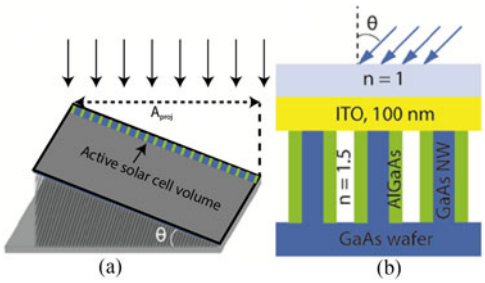

Fig. 1. (a) Schematic illustration of a solar cell measured under tilt angle of θ. (b) Schematic illustration of the defined structure for the simulation. For the simulation, instead of tilting the solar cell, the incoming light is tilted, that is, light is incident at an angle θ.

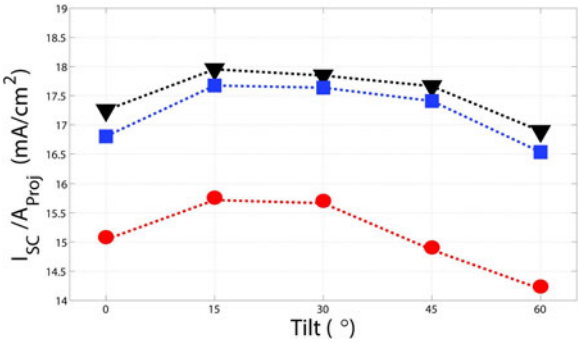

Fig. 2. Dependence of $I_{\rm SC}/A_{\rm proj}$ on the tilt angle θ for three different GaAs NW solar cells.

radial AlGaAs shell (20–40-nm shell thickness) at a temperature of 715 °C with Al/Ga molar flow ratio of 3.47. Secondary ion mass spectroscopy, performed on a planar layer grown with the same recipe, indicates 87% Al in the composition. To fabricate the solar cells, a partially planarized surface was then formed by depositing silicon oxide and spin-coating CYCLOTENE. To form the front contact, these layers were etched back to reveal the top of the NWs, the Au catalyst particles were removed, and, finally, an approximately 100-nm-thick indium tin oxide (ITO) top contact layer was deposited. Subsequently, on the substrate, multiple solar cells of 1 mm^2 in area were defined by patterning the ITO. The detailed description of the fabrication process is reported in [9].

A Newport ORIEL IQE 200 setup was used for external quantum efficiency (EQE) measurements. The *I–V* characteristics of the solar cells were measured at room temperature under the 1-sun AM1.5G spectrum of intensity $W_{\rm inc} = 1000\,{\rm W/m^2}$, using a Newport Sun simulator. The power conversion efficiency (η) was then obtained from $\eta = \frac{P_{\rm out}}{P_{\rm in}}$, where $P_{\rm out} = I_{\rm SC} * FF * V_{\rm OC}$ is the output power, and $P_{\rm in}$ is the incident power. For a tilted cell of area $A_{\rm cell}$, $P_{\rm in} = W_{\rm inc} * A_{\rm proj}$, with $A_{\rm proj} = \cos(\theta) * A_{\rm cell}$, where θ is the angle between the solar cell and the horizon as shown in Fig. 1(a) [note that this geometry configuration is equivalent to tilting the incidence angle by θ for a fixed cell, as shown in Fig. 1(b)]. Thus, the efficiency $\eta = I_{\rm sc}/A_{\rm proj} * FF * V_{\rm oc}/W_{\rm inc}$ is proportional to $I_{\rm SC}/A_{\rm proj}$. Conventionally, for an untilted cell with $\theta = 0$, the short-circuit current ($J_{\rm SC}$) is defined as $I_{\rm SC}$ divided by the cell area $A_{\rm cell}$. However, here, in the analysis of the performance of the tilted cells, we concentrate on this more relevant quantity $I_{\rm SC}/A_{\rm proj}$.

To aid in the analysis of the experimental results, optics simulation of the absorption of light was performed with the scattering matrix method [14]. In this method, the diffraction of light is modeled with Maxwell's equations. For the simulation, GaAs NW arrays were defined with the length, diameter, and pitch of 2800, 165, and 500 nm, respectively. Hundred-nanometer-thick ITO layer and a 40-nm-thick AlGaAs shell were introduced in the model. The incident medium is air with refractive index $n_{\rm incident} = 1$, and $n_{\rm filler} = 1.5$ is set for the filler between the NWs. In this modeling, the light is incident as a plane wave from a direction given by the angle θ with respect to normal incidence as shown in Fig. 1(b). To model the experimental case of unpolarized light, we averaged the results for transverse electric and transverse magnetic polarized light. Fig. 1(b) shows a schematic illustration of the defined structure for the simulation and the illumination direction.

The optical properties of the constituent materials are described with their respective wavelength-dependent refractive index. In [15]–[17], the refractive index of GaAs, AlGaAs, and ITO, respectively, have been discussed. We modeled the AlGaAs shell as $Al_{0.6}Ga_{0.4}As$. To simplify the modeling, we set the imaginary part of the refractive index of this AlGaAs to zero. With this approximation, we neglect a possible absorption of photons in the shell. Such absorption could have some effect on the total absorption in the high-energy ($\lambda < 500$ nm) region, where the AlGaAs shows strong direct optical transitions. However, for $\lambda > 500$ nm, we expect negligible absorption in the AlGaAs shell due to weak indirect optical transitions. In contrast, noticeable absorption in the ITO can, in principle, show up throughout the whole wavelength range, where the GaAs NW core absorbs, that is, for $\lambda < 870$ nm. Therefore, we included into the modeling the absorption losses in the ITO layer by using the complex-valued refractive index of the ITO.

III. Measured Dependence of Performance on Tilt Angle

We have measured the electrical properties of three GaAs NW solar cells fabricated on two different GaAs substrates for varying tilt angle with respect to the incident light, including the case of normally incident light, that is, for $\theta = 0$. It should be mentioned that the growth condition is not similar, and one of the samples (circle data points in the figures) has almost two times higher doping in the base than the other.

First, we concentrate on current, as measured by $I_{\rm SC}/A_{\rm proj}$ (see Fig. 2). The values that are reported in Fig. 2 for 0° tilt indeed indicate the $J_{\rm SC}$ values, which are 17.25, 16.8, and 15.04 mA/cm^2 for the triangle, square, and circle marked points, respectively. We find an increase of $I_{\rm SC}/A_{\rm proj}$ of $\approx 0.8\,{\rm mA/cm^2}$ (the average of the three samples) at 15° tilt angle relative to no tilt. The $I_{\rm SC}/A_{\rm proj}$ increase is ≈0.6 and 0.3 mA/cm^2 at 30° and 45° tilt angle, respectively. Interestingly, even at a tilt angle of 60°, 95% of the $I_{\rm SC}/A_{\rm proj}$ is retained compared with the normal incident condition providing experimental evidence that NW array solar cells are highly efficient at gathering diffuse or tilted incident light even at very high angles of incidence. Note that

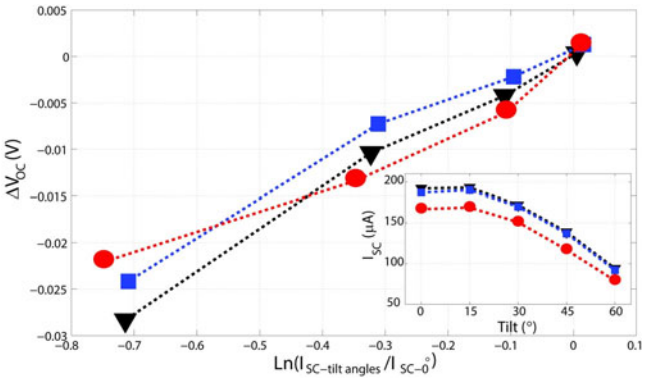

Fig. 3. Variation in V_{OC} (compared with the 0° tilt angle) with respect to the variation in measured current. The data points represent 15°, 30°, 45°, and 60° tilt angle from right to left, respectively. (Inset) Variation in I_{SC} with respect to the tilt angle from 0° to 60° tilt.

the absolute current output I_{SC} of the solar cell decreases with θ (see the inset in Fig. 3), as expected from the $\cos(\theta)$ dependence in the projected illumination area $A_{\mathrm{proj}} = A_{\mathrm{cell}} * \cos(\theta)$.

Next, we investigate the dependence of the voltage performance of the solar cell (see Fig. 3). We find a linear dependence of the open-circuit voltage (V_{OC}) as a function of $\ln(I_{\mathrm{SC}})$. Note that such a linear dependence indicates that the solar cell is characterized by an ideality factor n for operation around the open-circuit condition. In such a regime, the *I–V* curve is given by $I = I_{\mathrm{SC}} - I_0 \exp(qV/(nkT))$, from which, the V_{OC} is given by $V_{\mathrm{OC}} = \frac{nkT}{q}\ln(\frac{I_{\mathrm{SC}}}{I_0} - 1) \approx \frac{nkT}{q}\ln(\frac{I_{\mathrm{SC}}}{I_0})$, where n, k, T, q, and I_0 are the ideality factor, the Boltzmann constant, the temperature of the cell, the elementary charge, and the dark saturation current, respectively. Apart from I_{SC}, none of the other parameters are expected to depend on the illumination angle. Hence, we can define the variation in V_{OC} with respect to the zero tilt case as

$$\Delta V_{\mathrm{OC}} = V_{\mathrm{OC-tilt}} - V_{\mathrm{OC-0^\circ}} = \frac{nkT}{q}\ln\left(\frac{I_{\mathrm{SC-tilt}}}{I_{\mathrm{SC-0^\circ}}}\right)$$
$$= B * \ln\left(\frac{I_{\mathrm{SC-tilt}}}{I_{\mathrm{SC-0^\circ}}}\right) \quad (1)$$

where B is a constant. The measured ΔV_{OC} agrees well with this description, as seen from the linear increase of ΔV_{OC} with $\ln(\frac{I_{\mathrm{SC-tilt}}}{I_{\mathrm{SC-0\Delta}}})$ in Fig. 3. From linear fitting of the results in Fig. 3 to (1), we find an ideality factor of $n \approx 1.54$. When we instead turn to study the V_{OC} as a function of incidence angle [see Fig. 4(a)], we find for all three samples a noticeable drop at 60° tilt angle. From (1), we attribute this drop to the lower absolute current level I_{SC} (see the inset in Fig. 3), due to the decreased projected illumination area A_{proj} as discussed above. In contrast, the measured fill factor (*FF*) is nearly independent or possibly even slightly increasing with tilt angle [see Fig. 4(b)]. Such an increase in *FF* may be linked to the lower absolute current level, which could decrease resistive losses in the cell.

Finally, when turning to study the efficiency of the cells [see Fig. 4(c)], we find an increase by about 0.5% point in efficiency for all the three samples for $\theta = 15^\circ$ as compared with

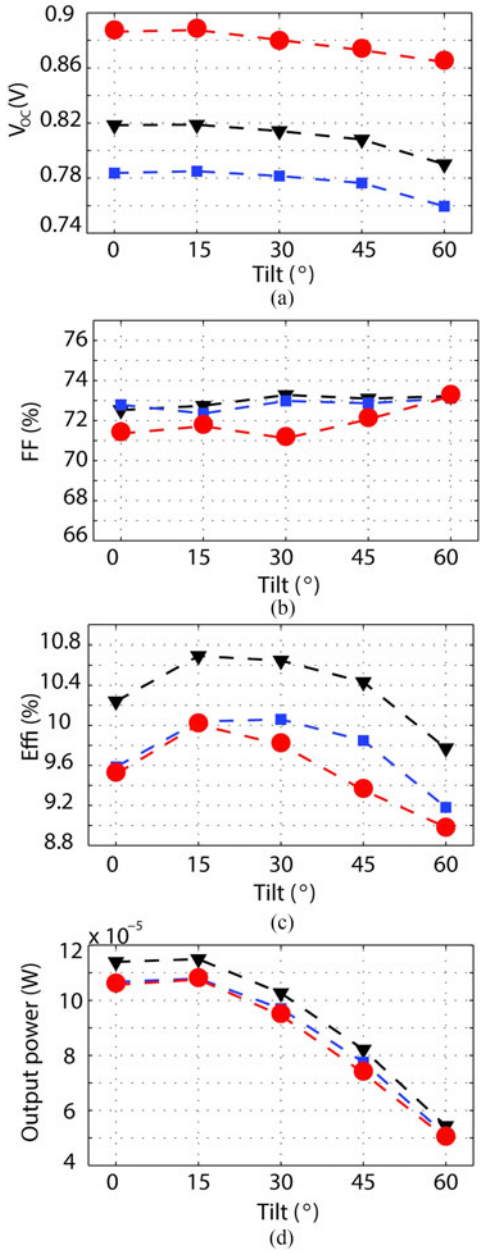

Fig. 4. Variation of (a) V_{OC}, (b) FF, (c) efficiency η, and (d) output power ($P_{\mathrm{out}} = I_{\mathrm{SC}} * FF * V_{\mathrm{OC}}$) at 1 sun with respect to the tilt angle from 0° to 60° tilt. The three datasets in each graph correspond to the three measured cells.

$\theta = 0^\circ$. It should be mentioned that the measured NW solar cell samples not only have higher efficiency (at 15° tilt angle) but also deliver higher actual output power [see Fig. 4(d)]. Thus, the increase in efficiency of an NW solar cell at the optimum tilt angle can more than fully compensate the loss in input power (due to the $\cos(\theta)$ factor from the tilting of the cell) and deliver higher output power (as compared with the 0° tilt).

It should be noted that for the case of a conventional crystalline silicon cell, or even for a black silicon solar cell, neither higher efficiency nor higher power is obtained for any tilt angle compared with normal incident light [18]. This unique property of NW array solar cells shows their potential for diffuse light

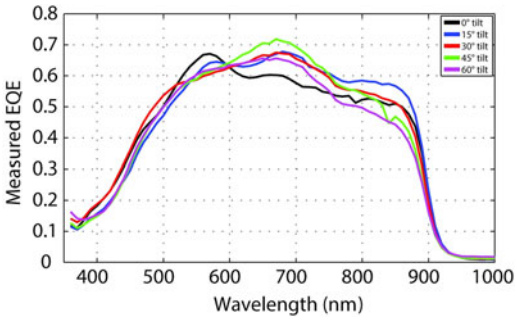

Fig. 5. Measured EQE for a GaAs NW solar cell with 500-nm pitch measured at 0–60° tilt angle. Higher EQE signal is measured in the red part of the spectrum (between ≈600 and 850-nm wavelengths) for almost all the tilt angles, as compared with the case of zero tilt.

illumination, as well as for practical fixed-installation conditions, where the illumination angle varies over the course of the day.

IV. Analysis of Current Generation Performance

Above, we saw that it is the strong photogeneration and charge-carrier extraction ability (as characterized by $I_{\rm SC}/A_{\rm proj}$) of the NW array solar cell at high tilted incidence that drives the increase in efficiency and even produces a slight increase in output power for a tilt angle of 15°. Here, to get a deeper understanding about the $I_{\rm SC}/A_{\rm proj}$ behavior, we have measured the EQE of the GaAs solar cell whose *I–V* characteristics are marked with triangles in Figs. 2–4. However, the EQE of the other two devices showed very similar trends. We performed the EQE analysis for varying tilt angle in steps of 15° up to $\theta = 60^{\circ}$ (see Fig. 5). For 0° tilt, we find a peak in the EQE at approximately $\lambda = 570$ nm in wavelength. The peak position shifts to 680-nm wavelength for all considered nonzero tilt angles. Moreover, for nonzero tilt, we identify two regions with different dependence compared with 0° tilt. First, relatively lower EQE signals are measured for wavelengths between ≈520 and 600 nm. Based on simulation results [see Fig. 6(b)], this could be attributed, for example, to the slightly increased reflection at these wavelengths for the case of nonzero tilt. Second, in the region between 610 and 850 nm, the EQE is improved for tilt angles in the range of 15–45°. Hence, we conclude that the higher measured $I_{\rm SC}/A_{\rm proj}$ at nonzero tilt angles of 15–45° in Fig. 2 is due to this increase in EQE in the long-wavelength part of the incident spectrum.

To understand this increase in the EQE at long wavelengths, we have simulated the optical response of the NW array with the scattering matrix method for varying incidence angle (see Section II for details). We present the fraction of light absorbed in the NWs [see Fig. 6(a)], the reflection back to the top air side [see Fig. 6(b)], and the transmission into the underlying substrate [see Fig. 6(c)]. It should be mentioned that we did not observe any considerable dependence of the in-plane rotation φ of the sample in the measurements. Similarly, no strong dependence of φ was noticed in the absorption modeling. Note that the results presented for the absorption modeling are for light incident in an incidence plane parallel to the high-symmetry

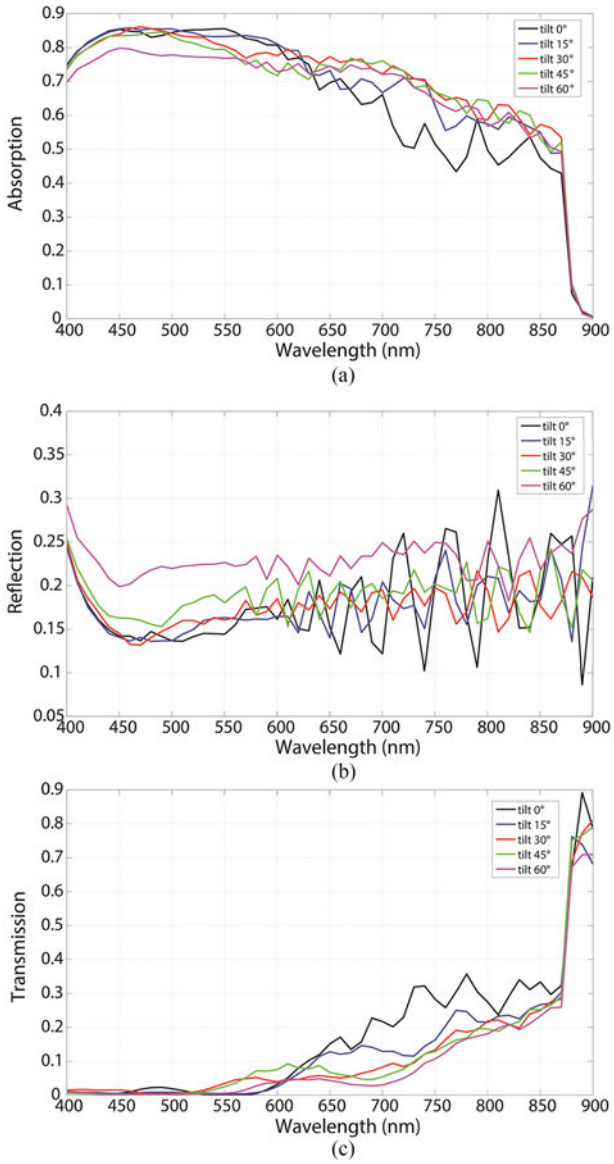

Fig. 6. Simulated (a) absorption, (b) reflection, and (c) transmission spectra of a GaAs NW array (NW length: 2800 nm, NW diameter: 160 nm, array pitch: 500 nm, $n_{\rm incident}$: 1, $n_{\rm filler}$: 1.5, and $n_{\rm substrate}$: GaAs) for different tilt angles. Note that all nonzero tilt angles lead to higher absorption than 0° tilt angle for wavelengths longer than 650 nm.

direction of the square lattice, where the NWs are separated by the 500 nm pitch.

The simulated absorption is enhanced for tilted incident light at wavelengths above 650 nm [see Fig. 6(a)], in line with the corresponding increase in the measured EQE of Fig. 5. The average reflection (between 600 and 850-nm wavelength) increases only slightly, from 18% to 22%, as the incidence angle is tilted from 0° to 60°. In contrast, the average transmission (between 600 and 850-nm wavelength) shows a much stronger dependence on the incidence angle and drops from 22% at $\theta = 0^{\circ}$ to 15% at $\theta = 15^{\circ}$, and to 12% for $\theta = 30^{\circ}$ and 45°. Hence, we deduce that by tilting the NW array, the reflection does not vary much, whereas the transmission reduces. Thus, the increased absorption in the

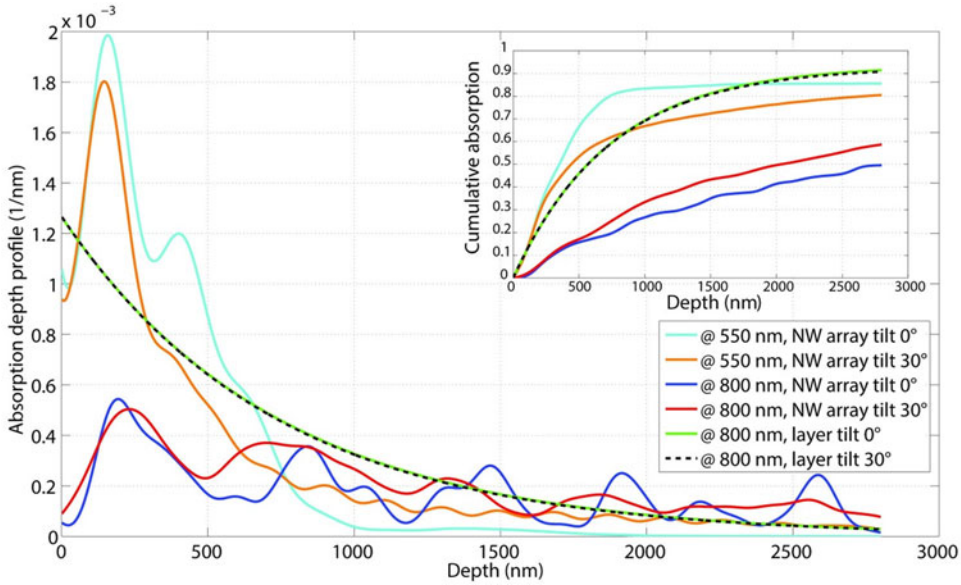

Fig. 7. Absorption depth profile for 550 and 800-nm wavelength for a GaAs NW array and for 800-nm wavelength for a GaAs layer at 0° and 30° tilted angle. (Inset) Corresponding cumulative absorption of the GaAs NW array and the layer.

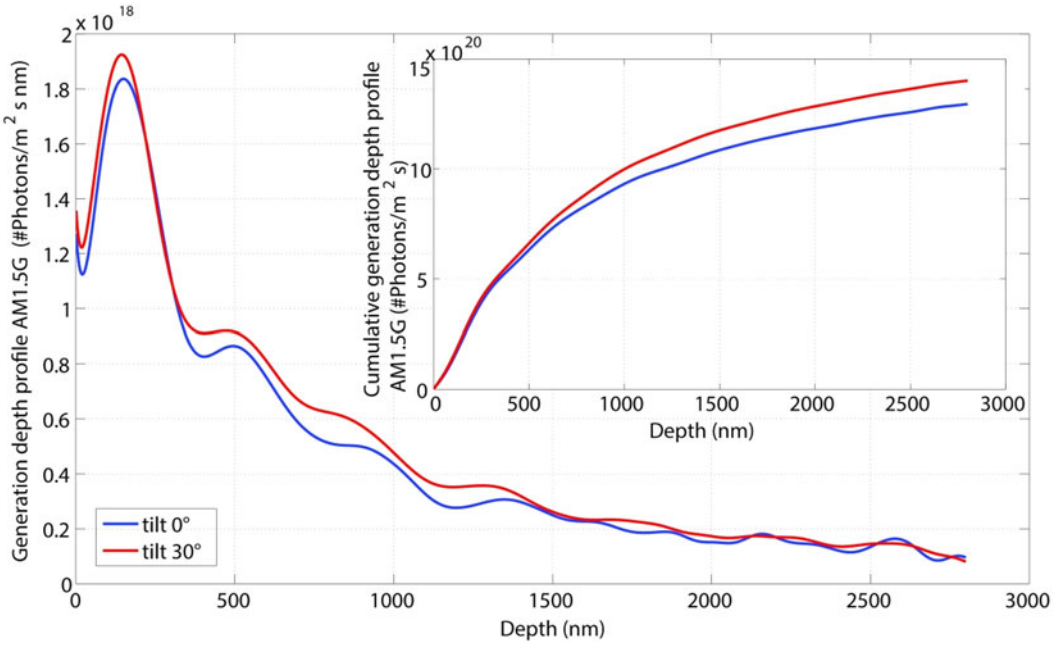

Fig. 8. Calculated photogeneration depth profile of GaAs NW array under AM1.5G illumination for 0° and 30° tilt. (Inset) Cumulative photogeneration for AM1.5G illumination. Between a depth of approximately 300 and 1400 nm, the AM1.5G absorption is higher for the tilted case, causing the cumulative absorption curves to diverge.

NW array decreases the amount of light that can transmit to the substrate.

To understand the absorption behavior even better, we have studied how the absorption is distributed along the axial direction of the NW, that is, with depth into the NW array. Fig. 7 shows such absorption depth profiles for 550 and 800-nm wavelength for 0° and 30° tilt (the corresponding cumulative absorption is shown in the inset). For comparison, we also show the absorption for a 2.8-μm-thick planar GaAs layer, which follows the Beer–Lambert law of exponential decay with depth into the layer. In contrast, the NW array shows a more complicated dependence with multiple peaks of varying periodicity.

Next, we relate the absorption depth profiles to the AM1.5G solar spectrum $I_{\mathrm{AM1.5}}(\lambda)$ used in the experiments. Note that we can translate the absorption depth profile $F(\lambda,\ z)$ into a photogeneration depth profile as $G_z(\mathrm{z}) = \int \mathrm{d}\lambda\ I_{\mathrm{AM1.5}}(\lambda)F(z,\lambda)/(2\pi\hbar c/\lambda)$ [13]. We show such photogeneration depth profiles for 0° and 30° incidence angle in

Fig. 8 (with the corresponding cumulative photogeneration profile in the inset). In the first 300 nm of depth along the NW length axis, the absorption is similar between the two cases. However, between 300 and 1400 nm, the cumulative photogeneration profiles for 0° and 30° tilt diverge (see the inset in Fig. 8), with a higher absorption for the tilted incidence. In the second half of the NW, from a depth of 1400 nm, the absorption is similar for both tilt angles, and the two cumulative photogeneration profiles are parallel. Quantitatively, the cumulative absorption is approximately 5% higher over the whole NW for the 30° tilt. Thus, the simulated absorption is higher in a 30° tilted NW array PV cell, qualitatively consistent with the measured increase in $I_{\rm SC}/A_{\rm proj}$ and the increase in efficiency. However, for a more complete analysis, not only the absorption but also the likelihood of collecting the photogenerated carriers should be considered.

For the current generation performance, in addition to the photogeneration rate, the probability to extract the photogenerated charges plays a major role. To assess the internal charge-carrier collection efficiency along the length of the NW, the electron beam-induced current (EBIC) response of a single NW was also measured, after the fabrication step of the AlGaAs shell, using the substrate as the back contact and the Au catalyst particle as the top contact. Such EBIC response is expected to be proportional to the probability to extract photogenerated charges. The EBIC response and the corresponding SEM micrograph of the measured NW are shown in Fig. 9(a) and (b), respectively. The relative EBIC profile at the center of the cross section of the wire, as a function of the length along the wire axis, is shown in Fig. 9(c). The profile consists of three regions with considerably different behavior:

1) n-type emitter region (of approximately ∼200 nm in length), which shows a sharply decreasing signal toward the Au tip of the NW, which we attribute to recombination of photogenerated holes (the minority carriers) in the Au particle or the contact [9];
2) a nearly flat and high response region (until ∼1500-nm depth), which we attribute to either charge separation by an electric field in a depletion region or diffusion in a quasi-neutral absorber characterized by a long diffusion length;
3) a last region (deeper than ∼1500-nm depth) near the base of the wire where the response decreases toward the substrate.

In this last region, we attribute the decrease in the response to a decreasing probability for electrons (the minority carriers) to diffuse to the depletion region with increasing distance from the depletion region. We note that the EBIC signal shows a drop when we shift with increasing radial position the electron beam to illuminate the surrounding shell. This drop indicates that electron–hole pairs generated in the shell show a lower probability to contribute to the EBIC signal than electron–hole pairs generated in the core.

To obtain the probability for charge extraction from this EBIC response, we assumed that the extraction probability is zero at the edge of the Au particle and 100% at the maximum point in the plateau region. After this, we convoluted this extraction

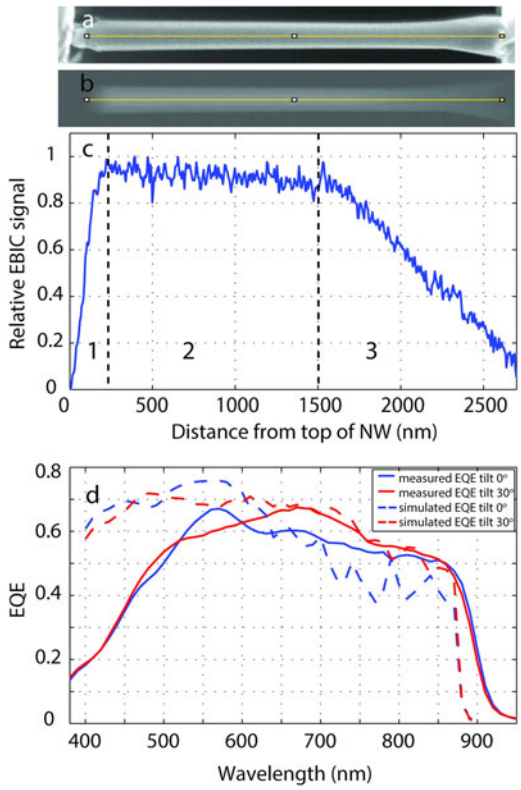

Fig. 9. (a) High-magnification SEM and (b) EBIC measurement of an NW grown similarly as the NWs in the measured NW array solar cells. The GaAs substrate and the Au particle are seen on the right and left edges of the images, respectively. (c) Measured EBIC profile along the center of the NW. (d) Measured (line) and simulated (dashed line) EQE signal for the normal incident and 30° tilted angle. The simulated EQE is calculated by multiplying the simulated wavelength-resolved photogeneration depth profile with the extraction probability profile [obtained from the EBIC profile shown in (c)].

profile with the simulated depth generation profile to yield a modeled EQE. We show the measured and modeled EQE for normal and 30° tilted incidence in Fig. 9(d). In agreement with measured data, a higher modeled EQE is found for 650–850-nm wavelengths for the 30° tilt compared with 0° tilt. By considering the measured EBIC profile [see Fig. 9(c)] and the calculated absorption depth profiles (see Fig. 7), it can be concluded that by tilting the NW array solar cell, the photogeneration increases in the region that shows a higher probability for extracting photogenerated carriers. This overlap of the regions for enhanced photogeneration and high extraction probability results in the observed increase in $I_{\rm SC}/A_{\rm proj}$.

The discrepancy between the measured and modeled EQE for wavelengths smaller than 550 nm, where the measured EQE drops faster than the modeled EQE, is attributed to absorption in the AlGaAs passivation layer. As discussed in Section II, such absorption was not included in the modeling for simplicity. We believe that in the experiments, a large fraction of the photogenerated charges in the AlGaAs shell recombine (due to lack of proper surface passivation of the shell), before transfer into the GaAs core where they could contribute to the current, leading to a drop in the measured EQE. Thus, increasing the Al concentration in the AlGaAs layer should further increase the $I_{\rm SC}$ of the NW array solar cell. Moreover, the ternary alloy $\rm Al_{\it x}In_{1-x}P$

grown on GaAs has been widely used as window/antireflection layer for multijunction solar cell, which can passivate GaAs well [19]. Hence, it could be used as an alternative to AlGaAs as well.

V. Conclusion

In summary, we have investigated the effect of tilted incidence on the electrical performance of GaAs NW array solar cells. Our measurements show that by tilting the NW array solar cells, stronger absorption can take place within the NWs as compared with normal incident light. Our modeling indicates on average a 5% higher absorption under AM1.5G for 30° tilt compared with at normal incidence. For the NWs in this study, this additional absorption occurs in a region of high probability to extract the photogenerated carriers, as shown by EBIC measurements on individual NWs. As an end result, the efficiency increases by approximately 1% (relative) for 30° tilt, compared with normal incidence. This enhanced absorption can, for small tilt angle, more than compensate for the decrease in the incoming power over the cell with increasing tilt. Indeed, we measure a small increase in actual power output when increasing the tilt to 15°. Furthermore, the efficiency of the NW array solar cell at 60° tilt is still 95% of the efficiency at normal incidence. The results indicate the prospect of NW array solar cells (compared with cells using planar absorber layers, even if textured) for delivering higher output power and consequently cheaper electricity generation.

References

[1] W. Shockley and H. J. Queisser, "Detailed balance limit of efficiency of p-n junction solar cells," *J. Appl. Phys.*, vol. 32, no. 3, pp. 510–519, 1961.

[2] B. M. Kayes *et al.*, "27.6% Conversion efficiency, a new record for single-junction solar cells under 1 sun illumination," in *Proc. 37th IEEE Photovoltaic Spec. Conf.*, 2011, pp. 4–8.

[3] M. A. Green *et al.*, "Solar cell efficiency tables (version 47)," *Prog. Photovoltaics, Res. Appl.*, vol. 24, no. 1, pp. 3–11, 2016.

[4] M. Zheng *et al.*, "III-Vs at scale: A PV manufacturing cost analysis of the thin film vapor–liquid–solid growth mode," *Prog. Photovoltaics, Res. Appl.*, vol. 24, pp. 871–878, 2016.

[5] J. Wallentin *et al.*, "InP nanowire array solar cells achieving 13.8% efficiency by exceeding the ray optics limit," *Science*, vol. 339, no. 6123, pp. 1057–1060, 2013.

[6] P. Krogstrup *et al.*, "Single-nanowire solar cells beyond the Shockley–Queisser limit," *Nature Photon.*, vol. 7, no. 4, pp. 306–310, 2013.

[7] Y. Cui *et al.*, "Efficiency enhancement of InP nanowire solar cells by surface cleaning," *Nano Lett.*, vol. 13, no. 9, pp. 4113–4117, 2013.

[8] G. Mariani *et al.*, "GaAs nanopillar-array solar cells employing *in situ* surface passivation," *Nature Commun.*, vol. 4, 2013, Art. no. 1497.

[9] I. Aberg *et al.*, "A GaAs nanowire array solar cell with 15.3% efficiency at 1 sun," *IEEE J. Photovoltaics*, vol. 6, no. 1, pp. 185–190, Jan. 2016.

[10] Y. Wu *et al.*, "Enhanced photovoltaic performance of an inclined nanowire array solar cell," *Opt. Exp.*, vol. 23, no. 24, pp. A1603–A1612, 2015.

[11] M. Heurlin *et al.*, "Continuous gas-phase synthesis of nanowires with tunable properties," *Nature*, vol. 492, no. 7427, pp. 90–94, 2012.

[12] N. Anttu *et al.*, "Absorption of light in InP nanowire arrays," *Nano Res.*, vol. 7, no. 6, pp. 816–823, 2014.

[13] J. Wallentin *et al.*, "InP nanowire array solar cells achieving 13.8% efficiency by exceeding the ray optics limit," *Science*, vol. 339, no. 6123, pp. 1057–1060, 2013.

[14] N. Anttu and H. Q. Xu, "Scattering matrix method for optical excitation of surface plasmons in metal films with periodic arrays of subwavelength holes," *Phys. Rev. B*, vol. 83, no. 16, 2011, Art. no. 165431.

[15] D. E. Aspnes and A. A. Studna, "Dielectric functions and optical parameters of Si, Ge, GaP, GaAs, GaSb, InP, InAs, and InSb from 1.5 to 6.0 eV," *Phys. Rev. B*, vol. 27, no. 2, 1983, Art. no. 985.

[16] D. E. Aspnes *et al.*, "Optical properties of $Al_xGa_{1-x}As$," *J. Appl. Phys.*, vol. 60, no. 2, 1986, Art. no. 754.

[17] Z. C. Holman *et al.*, "Infrared light management in high-efficiency silicon heterojunction and rear-passivated solar cells," *J. Appl. Phys.*, vol. 113, no. 1, 2013, Art. no. 013107.

[18] H. Savin *et al.*, "Black silicon solar cells with interdigitated back-contacts achieve 22.1% efficiency," *Nature Nanotechnol.*, vol. 10, no. 7, pp. 624–628, 2015.

[19] A. C. E. Chia *et al.*, "Electrical transport and optical model of GaAs-AlInP core-shell nanowires," *J. Appl. Phys.*, vol. 111, no. 9, 2012, Art. no. 094319.

Omid Madani Ghahfarokhi received the B.S. degree in electrical engineering-electronics and the M.Sc. degree in micro and nanotechnology from Neuchatel University, Neuchatel, Switzerland, in 2009, and the Ph.D. degree in physics from Oldenburg University, Oldenburg, Germany, in 2014.

His research has been primarily focused on semiconductor process integration such as amorphous and microcrystalline silicon solar cells, as well as silicon heterojunction solar cells. He is currently a Senior Device Engineer with Sol Voltaics AB, Lund, Sweden, working on the development of GaAs nanowire solar cells.

Nicklas Anttu received the M.S. degree in engineering physics from Umeå University, Umeå, Sweden, in 2007 and the Ph.D. degree in physics from Lund University, Lund, Sweden, in 2013.

His work has concentrated on the optical and electrooptical modeling of nanowire-array-based solar cells, with emphasis on optimizing the geometry and electrical design of the arrays for high efficiency.

Lars Samuelson received the Ph.D. degree from Lund University, Lund, Sweden, in 1977.

He then joined IBM as a Postdoctoral Fellow. In 1986, he became a Professor with Chalmers University, Gothenburg, Sweden. Since 1988, he has been a Professor with Lund University. In 1988, he founded the Lund Nanometer Structure Consortium, which today engages about 250 scientists. He is internationally recognized for his research on low-dimensional structures and the physics and applications thus made possible. He has authored about 600 articles and given more than 300 plenary/invited talks at international conferences (h-index 74).

Dr. Samuelson is a Fellow of the Institute of Physics, U.K., and the American Physical Society, as well as a Member of the Royal Swedish Academy of Sciences and the Royal Swedish Academy of Engineering Sciences. He is also Founder and CSO of Glo AB, Sol Voltaics AB, and Qunano AB. In 2008, he was appointed "Einstein Professor" by the Chinese Academy of Sciences. In 2013, he received the IUVSTA Prize for Science and, in 2014, the Fred Kavli Distinguished Lectureship in Nanoscience.

Ingvar Åberg (M'01) received the M.S. degree in engineering physics from Lund University, Lund, Sweden, in 2001 and the Ph.D. degree in electrical engineering and computer science from the Massachusetts Institute of Technology, Cambridge, MA, USA, in 2006. His graduate research was on hole transport in fully depleted strained silicon and strained silicon.germanium heterostructure on insulator MOSFETs.

Since joining Sol Voltaics AB, Lund, in 2011, he has held various positions relating to the development of III.V nanowire array photovoltaic cells. He is currently the Director of cell engineering, leading the company.s program on high-efficiency photovoltaics. Prior to joining Sol Voltaics AB, he held positions at other companies where he developed night vision complementary metal–oxide semiconductor imagers and silicon solar cells.